Microstructural Refinement and Corrosion Resistance Improvement of Heat-Treated A356 Alloy Processed by Equal Channel Angular Pressing

(Mikrostruktur Penghalusan dan Rintangan Kakisan Peningkatan Haba Dirawat A356 Aloi Diproses oleh Saluran Sama Sudut Menekan)

M.A. Gebril*, M.Z. Omar, N.K. Othman & I.F. Mohamed

ABSTRACT

The microstructure refinement, hardness and corrosion resistance of heat-treated A356 aluminium alloy processed by equal-channel angular pressing (ECAP) were investigated. ECAP was carried out at room temperature using a mold, with a channel angle of 120° via route A. Results of the investigation confirm that the flaky coarse silicon particles were effectively fragmented from 4.22 to 0.761 μm and the grain size reduced from 171 to 40 μm after four passes of heat-treated as-cast using ECAP process. ECAP processing increases the hardness of heat-treated as-cast alloy from 61 Hv to 125 HV after four passes. Heat-treated A356 alloy shows enhanced corrosion resistance from 0.0424 to 0.00149 mmy^{-1}, after four passes. In this research, ECAP processing has been shown to improve the hardness and corrosion resistance of as-cast A356 alloy.

Keywords: A356 aluminium alloy; corrosion rate; ECAP; grain size; heat treatment

ABSTRAK

Penghalusan mikrostruktur, kekerasan dan rintangan kakisan aloi aluminum A356 terawat haba yang diproses secara saluran sama sudut menekan (ECAP) dikaji. ECAP dilakukan pada suhu bilik dengan menggunakan acuan yang mempunyai sudut saluran 120° melalui laluan A. Keputusan kajian mengesahkan bahawa zarah silikon kasar berkeping terserpih dengan baik daripada 4.22 kepada 0.761 μm manakala saiz butiran berkurangan daripada 171 kepada 40 μm selepas empat laluan tuang terawat haba dengan menggunakan proses ECAP. Pemprosesan ECAP meningkatkan kekerasan aloi tuang terawat haba daripada 61 Hv kepada 125 HV selepas empat laluan. Aloi A356 terawat haba menunjukkan rintangan kakisan yang lebih baik, iaitu daripada 0.0424 kepada 0.00149 mmy^{-1} selepas empat laluan. Kajian ini telah menunjukkan bahawa pemprosesan ECAP telah meningkatkan kekerasan dan rintangan kakisan aloi A356 tuang.

Kata kunci: Aloi aluminium A356; ECAP; kadar kakisan ; rawatan haba; saiz butiran

INTRODUCTION

Primary dendritic α-Al phase and flaky silicon morphology are not desirable in certain applications of aluminium casting since they result in poor mechanical properties of Al-Si alloy. Coarse flake Si particles could initiate premature cracks during deformation. This reduces the workability of the alloy at room temperature, which in consequent reduces the ductility of the alloy (Haghdadi et al. 2012). The shape and distribution of Si particles have a strong influence on the electrochemical and mechanical properties of Al-Si alloy.

The cathodic behaviour of Si within the Al-rich matrix contributes to the occurrence of localized corrosion with the formation of micro-galvanic couples (Davis 2001), which in turn contributes to poor mechanical behavior such as in the stent applications (Galvin et al. 2017). A reduction in the area ratio of noble Si particles (cathode) to less-noble eutectic Al phase (anode) around Si particles significantly improve pitting corrosion resistance. In other words, smaller area ratio of cathode to anode (Ac/Aa) reduces the corrosion current density. The reduction in the size of

Si particles facilitates the repassivation of protective film (Fadavi & Tahamtan 2010) and the formation of passive film with better stability (Tahamtan & Fadavi 2009). The Al-Fe-Si-Mg compounds also behave cathodically with respect to the α-Al phase (Arrabal et al. 2013; Buarzaiga & Thorpe 1994; Mingo et al. 2016).

Heat treatment modifies the Si particles in such way that improves the strength of Al alloys through aging-hardening processes that occur as a result of the changes in the solubility of alloying elements in the matrix with temperature (Ghazali & Omar 2007; Mohamed & Samuel 2012). Heat treatment can be used to obtain the desired combination of mechanical properties (strength and ductility).

Severe plastic deformation (SPD) technique has the ability to effectively refine the grain structure to as small as an ultrafine micrometer-scale or nano-scale without any change in the cross-sectional dimensions of the sample. The major characteristics of SPD methods is the build-up of large plastic strain without any remarked change in the sample dimensions (Valiev et al. 2000). This technique is able to process ductile or brittle alloys to produce refined

grains (Mohamed et al. 2017). Equal channel angular pressing, ECAP, is considered to be the most appropriate SPD technique (Kumar et al. 2012; Valiev & Langdon 2006a, 2006b). During ECAP, intense plastic strain can be achieved through simple shear by pressing the sample through a die containing two intersecting channels of equal cross section (Kawasaki & Langdon 2011; Xu & Langdon 2003).

The material used in an ECAP is in the form of a rod or bar, and is pressed repetitively through a bent channel with an abrupt angle. This processing method can be easily carried out and has been effectively used to achieve grain refinement and improved mechanical properties for various metals and metallic alloys (Kawasaki et al. 2009; Xu et al. 2013).

ECAP has been used to improve corrosion resistance through microstructural refinement (Gebril et al. 2018; Sadawy & Ghanem 2016; Zheng et al. 2012). Additionally, several researchers have discovered that the grain refinement achieved through ECAP processing reduces the corrosion resistance of Al-Mg (Son et al. 2007) and pure Mg alloys (Song et al. 2010). Therefore, the present work was carried out to investigate the effect of microstructural refinement of heat-treated A356 aluminium alloy followed by ECAP processing and its impact on hardness and corrosion resistance.

MATERIALS AND METHODS

A commercial A356 aluminium alloy (Si- 6.7 wt. % Mg- 0.149 wt. % Fe- 0.126 wt. % Cu- 0.01 wt. % Mn- 0.002 wt. % Zn- 0.006 wt. % Cr- 0.001 wt. % Ti- 0.178 wt. %) were cast in ingot having initial dimensions of 80 mm × 40 mm × 140 mm (width × thickness × length). The sample was prepared for T6 heat treatment by heating at 535°C for 8 h followed by water quench and further aged at 180°C for 3 h (ASM Handbook Committee 1990; Gebril et al. 2018). Both as-cast and heat-treated as-cast samples were machined into a rod shape, with a diameter of 9.8 mm. The samples were processed by ECAP in a die channels having an inner angle, F of 120º and outer curvature, Y of 20º at room temperature using routes A (where the sample is not rotated between each pass). The microstructure features of the as-cast and heat-treated as-cast A356 were examined by optical microscope, FESEM and energy-dispersive X-ray spectroscopy (EDX). A Vickers hardness tester (micro Vickers hardness tester, Zwick, Germany; ZHVμ) was used to measure the hardness of the average of three samples per case. The microhardness test was according to ASTM E 384. All samples were extracted from the circular rods perpendicular to the pressing direction plane and ground through successive grades of silicon carbide abrasive papers of grit between 180 to 2000. The samples were further polished to a mirror like quality using diamond suspension down to 1 μm. Keller's reagent (1% HF, 1.5% HCl, 2.5% HNO3, H_2O) was used to show the constituents of the alloys. The scanning electron microscopy (SEM) images were recorded and elemental mapping was performed using EDX with a Zeiss (Merlin/

Merlin Compact/ Supra 55VP) microscope operated at an accelerated voltage of 15.00 kV.

Quantitative metallography analysis was carried out to measure the grain size according to ASTM E 112. The silicon particle size was measured using Smart Tiffv2 software considering at least 200 particles in each condition. The corrosion test was carried out at room temperature using a Gramry 3.2 potentiostat which was attached to a three-electrode that formed an electrochemical cell setup in a 3.5 wt. % NaCl solution was prepared as an electrolyte solution and used as a simulated environment for sea water typically exposed to different structures (Arrabal et al. 2013; Mingo et al. 2016). The measurements were carried triplicate times each experimental condition in separate experiments. The sample was mounted using Lecoset 7007 epoxy that was cured in air for 24 h before the test. The mounted test material having exposed surface area of 1 cm² to electrolyte was attached to the working electrode. A graphite electrode and a silver/silver chloride (Ag/AgCl) electrode (in 0.6 molL⁻¹ 3.5% NaCl solution) were used as a counter and reference electrodes, respectively. ASTM Standard G102-89 (2010) was used to provide guidance in electrochemical measurements of corrosion rates.

RESULTS AND DISCUSSION

Microstructure of A356 alloy pre/post T6 heat treatment Figure 1(a) illustrates the optical micrographs of the as-cast sample with typical hypoeutectic dendritic bright phase structure enclosed by dark Si eutectic phase. The dendritic grain measures approximately 171 μm with a coarse eutectic mixture phase. Figure 1(b) shows the eutectic Si particles in flake-like shape measuring approximately 4.22 μm in as-cast alloy. The eutectic Si particles, which were present due to the high cooling rate and low pouring temperature, surrounded the primary α-Al dendritic (Hirt et al. 1997; Legoretta et al. 2008; Saklakoğlu et al. 2011). The T6 heat treatment transform the flaky or lamellar morphology of Si particles into angular to spherical-shaped shown in Figure 1(c) and 1(d). In the solution heat treatment sample, the eutectic Si particles was fragmented and spheroidised during the coarsening processes, where the Si particles were refined and the edges have less sharp angles as in as-cast alloy prior to heat treatment even though a significant amount of acicular-shaped particles remained after the T6 heat treatment process (Li et al. 2011; Ogris et al. 2002; Tiryakioğlu 2008).

MICROSTRUCTURE OF ECAP PROCESSING

Figure 2 shows the optical and SEM micrographs of ECAPed as-cast after two passes, for pre T6 (a, b) and heat-treated samples (c, d), respectively. In the initial stage of ECAP, the resulting deformation shear bands rapidly subdivide the coarse grains of the as-cast alloy. After two passes route A (where the sample is not rotated between each pass), the primary α-Al grain size of the Al−Si alloy become elongated, with some grains being more elongated
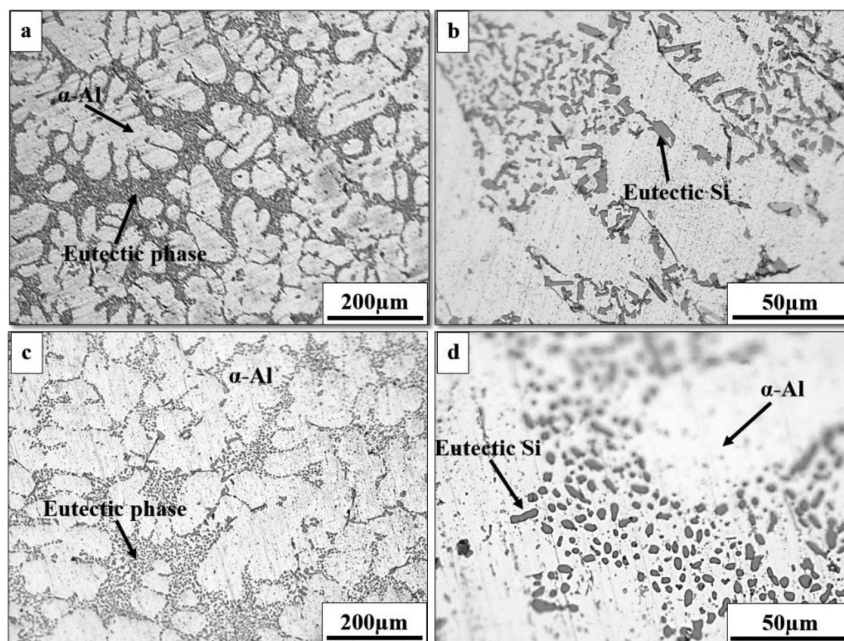
FIGURE 1. Microstructure of A356 alloy pre T6 (a) as-cast sample (b) enlarged image of Si morphology, post T6 (c) as- cast, and (d) enlarged image of Si morphology
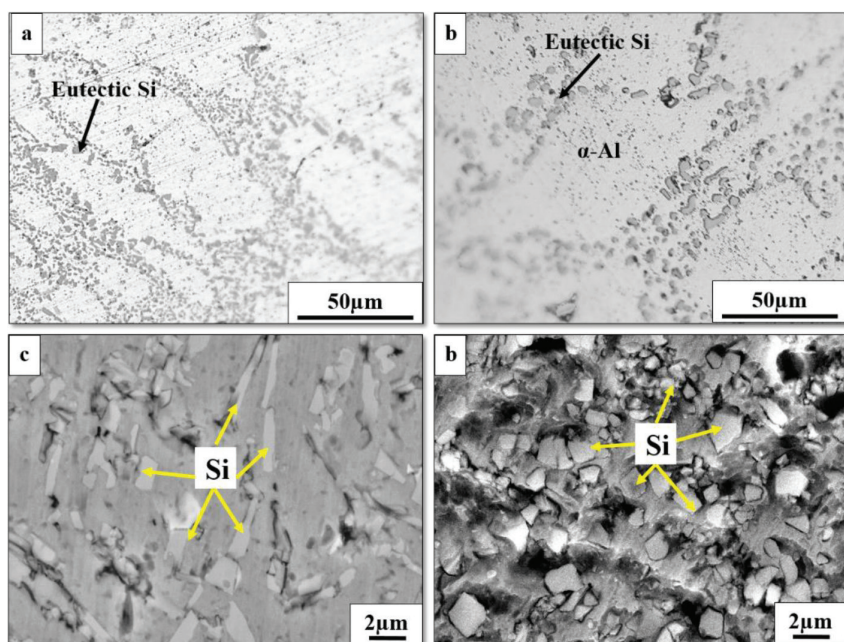

FIGURE 2. Optical micrographs of ECAPed samples after two passes (a) as-cast (b) heat treated as-cast while (c) and (d), their respected SEM micrograph

and grain boundaries likely to be position at around 45°. The microstructure is relatively inhomogeneous and the eutectic phase is randomly distributed in the matrix. During the second pass, the grains within the as-cast and heat-treated as-cast samples were greatly reduced from the initial size of ~171 μm to ~105.1 and 62.85 μm, respectively. Figure 2(c), 2 (d) and Table 1 shows the Si particles that had been fragmented and refined after two passes of ECAP and the eutectic phase can be seen to be

finer in heat-treated sample. However, as for the α-Al phase, the effect of straining from the two ECAP passes had transformed them into elongated grains. The average grain and Si particle size are presented in Table 1.

Figure 3 shows the optical and SEM micrographs of Si morphology of the ECAPed as-cast (a, c) and heat-treated as-cast samples (b, d) A356 alloy after four passes. Applying greater strain resulted in the primary α-Al phase and eutectic constituents being elongated into a plate-like

TABLE 1. Average values of α-Al grain and Si size of ECAPed A356 alloy, route A

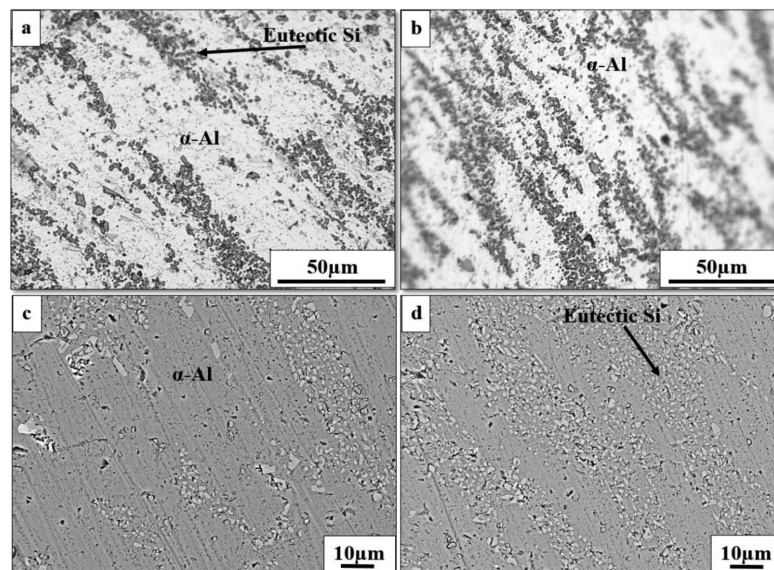| Pass No. Route	Si particles size (μm)	α-Al grains size (μm)
As-cast	4.22	171
As-cast,2 pass0	2.68	105.10
Heat-treated as-cast, 2 pass	1.74	62.85
As-cast,4 pass	0.98	47.05
Heat-treated as-cast, 4 pass	0.761	40.40
Pass No. Route	Si particles size (μm)	α-Al grains size (μm)

FIGURE 3. Optical and SEM micrographs of ECAPed A356 alloy after 4 passes (a) as-cast (b) heat-treated as-cast while (c) and (d), their respected SEM micrograph

shape in both alloy samples. The Si particles and the eutectic are finer in contrast when compared with the two-pass samples due to fragmentation of Si particles, as also discussed by the previous work of Zhilyaev and Ruano (2011).

The Si particles in the heat-treated sample are more refined and more homogenously distributed due to the dual effect of spheroidisation of Si particles resulting from heat treatment and the fragmentation of eutectic Si particles as a consequence of the ECAP process. Compared to the Si particles and eutectic phase distribution subjected to ECAP process, the particles in the ECAPed heat-treated samples appeared to be finer than those in the ECAPed as-cast samples. The primary α-Al phase in ECAPed heat-treated sample are finer. However, in this study, the spheroidisation and fragmentation of the Si particle are due to the T6 heat treatment followed by ECAP process. Subjecting as-cast A356 alloy to ECAP process via route A resulted in a morphological change of the primary α-Al from dendritic to longitudinal shape while the morphology of the Si particles disintegrates from coarse flakes into small fragments that are uniformly distributed along the grain boundaries.

HARDNESS OF A356 AFTER ECAP

Figure 4 demonstrates the Vickers microhardness of as-cast and heat-treated as-cast samples measured after combination with ECAP processing via route A. The spheroidisation of eutectic Si after T6 heat treatment increase the hardness of samples. The microhardness of the sample subject to T6 increased from 61 to 75 Hv. The spheroidisation of Si particles after T6 heat treatment and precipitation of magnesium silicide (Mg_2Si) particles during aging process tend to increase the ultimate tensile strength as well as hardness (Möller et al. 2012; Zhu 2017).

Since shear force could break down the dendrite arms of the α-Al phase and cause grain refinement, the value of microhardness increases with increasing ECAP pass number. Moreover, the brittle and hard eutectic Si particles might break during deformation, and with further deformation their mean free space could be further reduced. Since strength of materials is inversely related to the free space of particles, the hardness of the samples increases with increasing the pass number (Gebril et al. 2019; Haghshenas et al. 2009a, 2009b). Thus, the application of high strain results in increased hardness of the A356 alloy due to increased fragmentation of the eutectic Si particles and
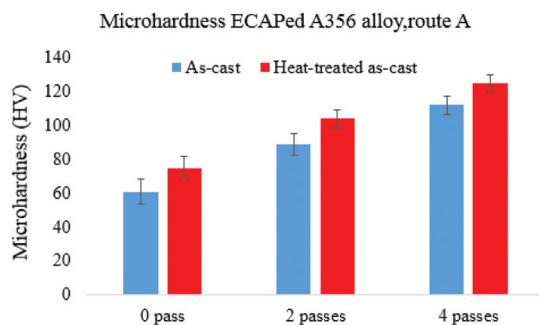
FIGURE 4. Microhardness of ECAPed as-cast and heat-treated
A356 processing by route A

reduced grain size in addition to the increase in density of dislocation. As has been reported by earlier studies, the high strain induced in a material during the ECAP process increases both dislocation density and grain refinement (Goodarzy et al. 2014; Kumar et al. 2012; Zhilyaev & Ruano 2011). The resulting finer eutectic Si improve the mechanical properties of the semisolid A356 (Sherif et al. 2011). However, the effect of the intermetallic compounds is a secondary effect.

PITTING CORROSION

Surface morphology Figure 5(a) to 5(c) shows the corroded surface appearance of as-cast, ECAPed as-cast after four passes and ECAPed heat-treated as-cast after four pass of route A and after corrosion in 3.5% NaCl solution. Visual investigation of the corroded surface of three samples shows the corrosion occurs in the eutectic phase area while the α-Al phase remains unattacked. Generally, the number and size of the pits as well as the large clear area around the pits of ECAPed heat-treated samples, are smaller than those in the ECAPed as-cast and as-cast samples due to the reduction and redistribution of

cathodic phases after the heat treatment and ECAP process. The bigger and deeper the pits, the more stable they are, and should be avoided (Son et al. 2007). The presence of corrosion free area around the pits indicate that anodic reactions occur within the pit due to concentration of galvanic cells while the cathodic reactions occur in this surrounding corrosion-free area (Callister Jr. & Rethwisch 2012).

The application of strain during the ECAP process had resulted in reduced grain size and development of crystalline defects, including dislocations of the grain boundary. An increase in grain boundary area and dislocations had resulted in the formation of passive films and hence, the corrosion resistance of ultrafine grains improved by the rapid formation of passive films at surface crystalline defects, including grain boundaries and dislocations (Balyanov et al. 2004; Boag et al. 2011; Wang et al. 2015). The grain boundaries and residual stresses effect depends on the nature of corrosion environment. If the corrosion process progresses by active anodic dissolution, then grain boundaries will accelerate the corrosion rate. In contrast, if the system undergoes passivation, then the grain boundaries will facilitate the passivation process and thereby reduce the corrosion rate (Ahmadkhaniha et al. 2017; Ralston et al. 2010). The microstructure refinement through ECAP processing improves the corrosion resistance of Al-Si alloy (Arrabal et al. 2013; Mingo et al. 2016), Ti alloy (Balyanov et al. 2004) and Cu alloy (Miyamoto et al. 2008).

Potentiodynamic Test Based on a simulation of sea water, 3.5% NaCl electrolyte solution at room temperature (Yahya & Rahim 2011) was used to evaluate the electrochemical behavior of as-cast, ECAPed as-cast and heat-treated as-cast A356 alloy by exposing the samples to a corrosive environment. The rate of corrosion was measured using the linear polarization technique through the Tafel
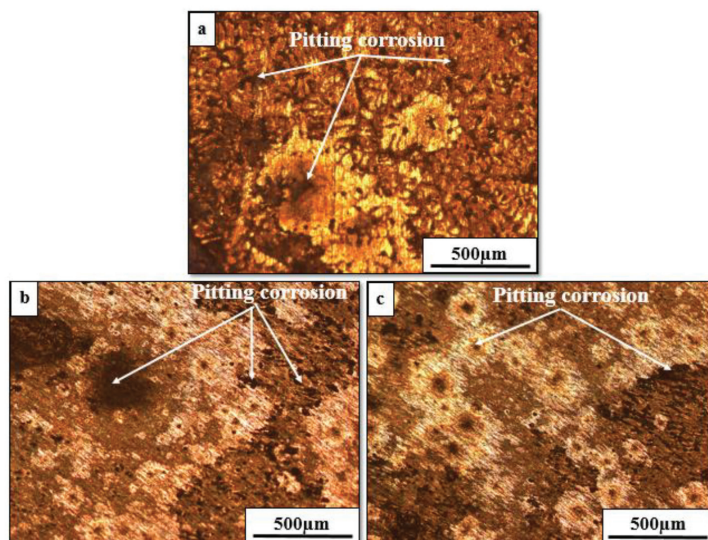

FIGURE 5. Pitting corrosion of A356 alloy in 3.5 wt. % NaCl solution (a) as-cast, (b) as-cast
after 4 ECAP passes and (d) heat-treated as-cast after 4 ECAP passes

extrapolation method to establish the corrosion resistance of the three samples. Figure 6 and Table 2 show how microstructure refinement influence the corrosion resistance of A356 alloy in 3.5 wt. % NaCl solution.

Based on the curves shown in Figure 6, the lower corrosion rate and higher polarization resistance of the heat-treated as-cast sample could be attributed to the modification in the shape of certain Si particles, where these particles became substantially finer after heat treatment followed by ECAP process. Hence, the enhanced corrosion resistance is believed to be associated with the following factors: A reduction in the area ratio between the cathodic and anodic phases due to refinement and spheroidisation of Si particles; precipitation of Mg_2Si phase that have anodic action with regard to the Al matrix, which may enhance localized corrosion (Yasakau et al. 2007) after heat treatment; fragmentation and homogenisation of Si particles (Ogris et al. 2002) after the ECAP process. The corrosion rate of the as-cast alloy was 0.042 mmy^{-1}, reduced to 0.00173 and 0.00148 mmy^{-1} after ECAPed as-cast and heat-treated as-cast A356 alloy, respectively. The polarization resistance depends on the microstructural state. After the ECAP process, the polarization resistance for as-cast and heat-treated as-cast samples increased with more ECAP passes. Nevertheless, after the ECAP process, the polarization resistance for the A356 alloy was found to be inferior to that of the as-cast sample, which positively affected the reconstruction of the metal protective layer, as shown in Table 2. However, the rate of corrosion of the as-cast and heat-treated as-cast decreased with more ECAP passes.

PITTING CORROSION APPEARANCE

Figure 7 shows a side view of the pitting corrosion of A356 alloy. Figure 7(a) to 7(c) shows the pitting corrosion of (a) the as-cast, (b) ECAPed as-cast after four passes and (d) ECAPed heat-treated as-cast after four passes of A356 alloy samples. The presence of the enlarged eutectic mixture phase area in the as-cast sample, as shown in Figure 7(a) would eventually result in a wider area of corrosion on the surface of alloy compared to four passes ECAPed as-cast and heat-treated samples. The microgalvanic corrosion between eutectic Si and Al matrix could contribute to the occurrence of pitting corrosion within the area that contains high Si impurities. The depth of corrosion in the eutectic mixture phase for both ECAPed as-cast with heat-treated as-cast samples, was evident. The refined grains in an elongated shape, the reduction in the size of Si particles and the distribution of eutectic phase resulted in lower corrosion rate of ECAPed heat-treated as-cast alloy sample compared to that of the as-cast alloy sample, as can be seen in Figure 7 and Table 2.

CONCLUSION

In this study, the impact of microstructural refinement on the hardness and corrosion resistance of A356 alloy
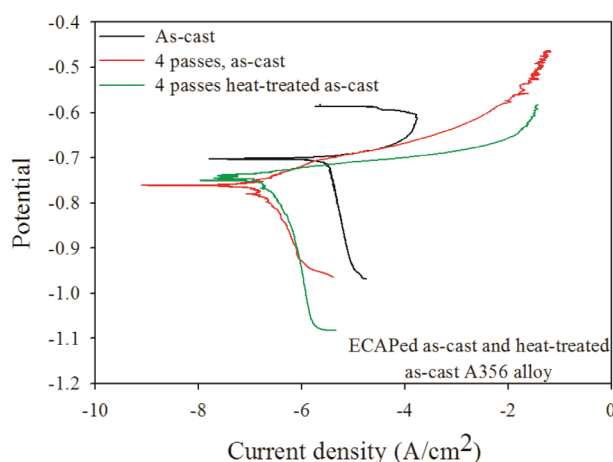

FIGURE 6. Polarization curves of (a) as-cast and ECAPed, 4 passes (b) as-cast and (c) heat-treated as-cast of A356 alloy

TABLE 2. Average values of current density (Icorr.), polarization resistance (Rp) and corrosion rate (CR) of A356 alloy before and after ECAP process

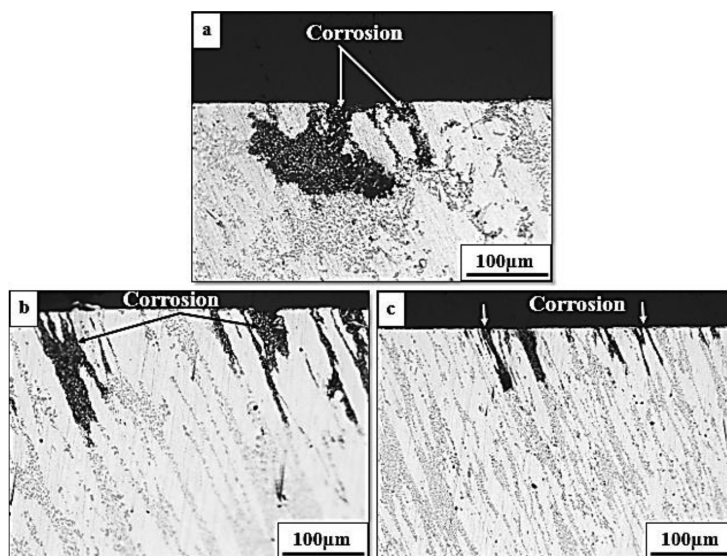| Pass No. Route	$E_{corr.}$ (V)	$I_{corr.}$ (A/cm^2)	Rp (Ω.cm^2)	CR (mmy^{-1})
0 pass	-0.703	3.894×10^{-6}	5.215×10^3	0.0424
As-cast, 4 pass	-0.761	1.583×10^{-7}	9.020×10^4	0.00173
Heat-treated as-cast, 4 pass	-0.745	1.369×10^{-7}	9.026×10^4	0.00149

FIGURE 7. Pitting corrosion of A356 alloy in 3.5 wt. % NaCl solution (a) as-cast, (b) as-cast cast after 4 ECAP passes and (d) heat-treated as-cast after 4 ECAP passes

processed by a combination of heat treatment and ECAP process via route A, was investigated. The following conclusions are made.

ECAP processing enables microstructure refinement through increased dislocation density, reduction of grain and Si sizes, redistribution of eutectic phase, and reduction of cathodic area sites. Each of these microstructural change plays an important role in increasing the hardness, reducing corrosion rate and increasing the polarization resistance by reducing the area ratio of cathode to anode (Ac/Aa) in microgalvanic affect. A fine-grained structure with a greater grain boundary area reduces the concentration chloride per grain boundary area, thereby reducing current density. The combination of heat treatment and ECAP accords low current density of $1.369\times10^{-7}A/cm^2$ to the A356 alloy when 3.5 wt. % NaCl solution was used. The enhanced corrosion resistance can be attributed to the refined Si particles which impeded the occurrence of microgalvanic cells in the protective layer of the alloy surface.

ECAP process is one of the most effective methods for producing ultrafine grained bulk materials having better corrosion resistance and hardness by refining the grains and enhancing the distribution of eutectic mixture throughout the material.

REFERENCES

Ahmadkhaniha, D., Fedel, M., Sohi, M.H. & Deflorian, F. 2017. Corrosion behavior of severely plastic deformed magnesium based alloys: A review. *Surface Engineering and Applied Electrochemistry* 53(5): 439-448.

Argade, G.R., Panigrahi, S.K. & Mishra, R.S. 2012. Effects of grain size on the corrosion resistance of wrought magnesium alloys containing neodymium. *Corrosion Science* 58: 145-151. doi:10.1016/j.corsci.2012.01.021.

Arrabal, R., Mingo, B., Pardo, A., Mohedano, M., Matykina, E. & Rodríguez, I. 2013. Pitting corrosion of rheocast A356 aluminium alloy in 3.5wt.% NaCl solution. *Corrosion Science* 73: 342-355. doi:10.1016/j.corsci.2013.04.023.

ASM Handbook Committee. 1990. *ASM Metals Handbook, Vol 02. Properties and Selection: Nonferrous Alloys and Special-Purpose Materials*. ASM International. pp. 3330-3345. doi:10.1016/S0026-0576(03)90166-8.

Balyanov, A., Kutnyakova, J., Amirkhanova, N.A., Stolyarov, V.V., Valiev, R.Z., Liao, X.Z., Zhao, Y.H., Jiang, Y.B., Xu, H.F., Lowe, T.C. & Zhu, Y.T. 2004. Corrosion resistance of ultra fine-grained Ti. *Scripta Materialia* 51(3): 225-229. doi:10.1016/j.scriptamat.2004.04.011.

Boag, A., Hughes, A.E., Glenn, A.M., Muster, T.H. & McCulloch, D. 2011. Corrosion of AA2024-T3 Part I: Localised corrosion of isolated IM particles. *Corrosion Science* 53(1): 17-26. doi:10.1016/j.corsci.2010.09.009.

Buarzaiga, M.M. & Thorpe, S.J. 1994. Corrosion behavior of as-cast, silicon carbide particulate-aluminum alloy metal-matrix composites. *Corrosion* 50(3): 176-185.

Davis, J.R. 2001. Aluminum and aluminum alloys. In *Light Metals and Alloys*. doi:10.1361/autb2001p351. pp. 351-416.

Fadavi Boostani, A. & Tahamtan, S. 2010. Effect of a novel thixoforming process on the microstructure and fracture behavior of A356 aluminum alloy. *Materials and Design* 31(8): 3769-3776. doi:10.1016/j.matdes.2010.03.019.

Galvin, E., O'Brien, D., Cummins, C., Mac Donald, B.J. & Lally, C. 2017. A strain-mediated corrosion model for bioabsorbable metallic stents. *Acta Biomaterialia* 55(9): 505-517. doi:10.1016/j.actbio.2017.04.020.

Gebril, M.A., Omar, M.Z., Mohamed, I.F., Othman, N.K. & Abdelgnei, M.A.H. 2018. Corrosion improvement and microstructure evaluation of sem-solid A356 alloy by ECAP process. *Journal of Physics: Conference Series*. Vol. 1082: 12110.

Gebril, M.A., Omar, M.Z., Othman, N. & Mohamed, I.F. 2019. Effect of equal channel angular pressing processing routes on corrosion resistance and hardness of heat treated A356 alloy. *Sains Malaysiana* 48(3): 661-668.

Ghazali, M.J., Ghani, J.A. & Omar, M.Z. 2007. Plastic deformation characteristics of worn precipitation-hardened aluminium alloys. *International Journal of Mechanical and Materials Engineering* 2(2): 125-129.

Goodarzy, M.H., Arabi, H., Boutorabi, M.A., Seyedein, S.H. & Najafabadi, S.H.H. 2014. The effects of room temperature ECAP and subsequent aging on mechanical properties of 2024 Al alloy. *Journal of Alloys and Compounds* 585: 753-759. doi:10.1016/j.jallcom.2013.09.202.

Haghdadi, N., Zarei-Hanzaki, A., Abedi, H.R. & Sabokpa, O. 2012. The effect of thermomechanical parameters on the eutectic silicon characteristics in a non-modified cast A356 aluminum alloy. *Materials Science and Engineering A* 549: 93-99. doi:10.1016/j.msea.2012.04.010.

Haghshenas, M., Zarei-hanzaki, A. & Sabetghadam, H. 2009a. The room temperature mechanical properties of a thermo-mechanically processed Thixocast A356 aluminum alloy. *Journal of Alloys and Compounds* 477(1-2): 250-255. doi:10.1016/j.jallcom.2008.10.090.

Haghshenas, M., Zarei-hanzaki, A. & Jahazi, M. 2009b. An investigation to the effect of deformation-heat treatment cycle on the eutectic morphology and mechanical properties of a Thixocast A356 alloy. *Materials Characterization* 60(8): 817-823. doi:10.1016/j.matchar.2009.01.020.

Hirt, G., Cremer, R., Witulski, T. & Tinius, H.C. 1997. Lightweight near net shape components produced by thixoforming. *Materials & Design* 18(4-6): 315-321. doi:10.1016/S0261-3069(97)00071-X.

Kawasaki, M., Figueiredo, R.B. & Langdon, T.G. 2011. An investigation of hardness homogeneity throughout disks processed by high-pressure torsion. *Acta Materialia* 59(1): 308-316. doi:10.1016/j.actamat.2010.09.034.

Kawasaki, M., Horita, Z. & Langdon, T.G. 2009. Microstructural evolution in high purity aluminum processed by ECAP. *Materials Science and Engineering: A* 524(1-2): 143-150. doi:10.1016/j.msea.2009.06.032.

Kumar, S.R., Gudimetla, K., Venkatachalam, P., Ravisankar, B. & Jayasankar, K. 2012. Microstructural and mechanical properties of Al 7075 alloy processed by Equal Channel Angular Pressing. *Materials Science and Engineering: A* 533: 50-54. doi:10.1016/j.msea.2011.11.031.

Legoretta, E.C., Atkinson, H.V. & Jones, H. 2008. Cooling slope casting to obtain thixotropic feedstock II: Observations with A356 alloy. *Journal of Materials Science* 43(16): 5456-5469. doi:10.1007/s10853-008-2829-1.

Li, B., Wang, H., Jie, J. & Wei, Z. 2011. Effects of yttrium and heat treatment on the microstructure and tensile properties of Al-7.5Si-0.5Mg alloy. *Materials and Design* 32(3): 1617-1622. doi:10.1016/j.matdes.2010.08.040.

Mingo, B., Arrabal, R., Pardo, A., Matykina, E. & Skeldon, P. 2016. 3D study of intermetallics and their effect on the corrosion morphology of rheocast aluminium alloy. *Materials Characterization* 112: 122-128. doi:10.1016/j.matchar.2015.12.006.

Miyamoto, H., Harada, K., Mimaki, T., Vinogradov, A. & Hashimoto, S. 2008. Corrosion of ultra-fine grained copper fabricated by equal-channel angular pressing. *Corrosion Science* 50(5): 1215-1220. doi:10.1016/j.corsci.2008.01.024.

Mohamed, A.M.A. & Samuel, F.H. 2012. A Review on the heat treatment of Al-Si-Cu/Mg casting alloys. In *Heat Treatment - Conventional and Novel Applications. InTech.* pp. 55-72. doi:10.5772/2798.

Mohamed, I.F., Masuda, T., Lee, S., Edalati, K., Horita, Z., Hirosawa, S., Matsuda, K., Terada, D. & Omar, M.Z. 2017. Strengthening of A2024 alloy by high-pressure torsion and subsequent aging. *Materials Science and Engineering: A* 704: 112-118. doi:10.1016/j.msea.2017.07.083.

Möller, H., Govender, G. & Stumpf, W. 2012. Factors influencing tensile mechanical properties of Al-7Si-Mg casting alloys A356/7. In *Light Metals,* edited by Suarez, C.E. Germany: Springer. pp. 467-471.

Ogris, E., Wahlen, A., Lüchinger, H. & Uggowitzer, P.J. 2002. On the silicon spheroidization in Al-Si alloys. *Journal of Light Metals* 2(4): 263-269. doi:10.1016/S1471-5317(03)00010-5.

Ralston, K.D., Birbilis, N. & Davies, C.H.J. 2010. Revealing the relationship between grain size and corrosion rate of metals. *Scripta Materialia* 63(12): 1201-1204.

Sadawy, M.M. & Ghanem, M. 2016. Grain refinement of bronze alloy by equal-channel angular pressing (ECAP) and its effect on corrosion behaviour. *Defence Technology* 12(4): 316-323. doi:10.1016/j.dt.2016.01.013.

Saklakoğlu, N., Gencalp, S., Kasman, Ş. & Saklakoğlu, İ.E. 2011. Formation of globular microstructure in A380 aluminum alloy by cooling slope casting. *Advanced Materials Research* 264-265: 272-277. doi:10.4028/www.scientific.net/AMR.264-265.272.

Sherif, E.M., Almajid, A.A., Latif, F.H. & Junaedi, H. 2011. Effects of graphite on the corrosion behavior of aluminum - Graphite composite in sodium chloride solutions. *International Journal of Electrochemical Science* 6: 1085-1099.

Son, I.J., Nakano, H., Oue, S., Kobayashi, S., Fukushima, H. & Horita, Z. 2007. Pitting corrosion resistance of anodized aluminum alloy processed by severe plastic deformation. *Materials Transactions* 48(1): 21-28. doi:10.2320/matertrans.48.21.

Song, D., Ma, A. Bin, Jiang, J., Lin, P., Yang, D. & Fan, J. 2010. Corrosion behavior of equal-channel-angular-pressed pure magnesium in NaCl aqueous solution. *Corrosion Science* 52(2): 481-490. doi:10.1016/j.corsci.2009.10.004.

Tahamtan, S. & Fadavi Boostani, A. 2010. Microstructural characteristics of thixoforged A356 alloy in mushy state. *Transactions of Nonferrous Metals Society of China* (English Edition) 20(SUPPL. 3): s781-s787. doi:10.1016/S1003-6326(10)60581-X.

Tahamtan, S. & Fadavi Boostani, A. 2009. Quantitative analysis of pitting corrosion behavior of thixoformed A356 alloy in chloride medium using electrochemical techniques. *Materials and Design* 30(7): 2483-2489. doi:10.1016/j.matdes.2008.10.003.

Tiryakioğlu, M. 2008. Si particle size and aspect ratio distributions in an Al-7%Si-0.6%Mg alloy during solution treatment. *Materials Science and Engineering: A* 473(1-2): 1-6. doi:10.1016/j.msea.2007.03.044.

Valiev, R.Z. & Langdon, T.G. 2006a. Developement in the use of ECAP processing fro grain refinement. *Reviews on Advanced Materials Science* 13: 15-26. http://wwwproxy.ipme.ru/e-journals/RAMS/no_11306/valiev.pdf.

Valiev, R.Z. & Langdon, T.G. 2006b. Principles of equal-channel angular pressing as a processing tool for grain refinement. *Progress in Materials Science* 51(7): 881-981. doi:10.1016/j.pmatsci.2006.02.003.

Valiev, R.Z., Islamgaliev, R.K. & Alexandrov, I.V. 2000. Bulk nanostructured materials from severe plastic deformation. *Prog. Mat. Sci.* 45: 103-189.

Wang, X., Nie, M., Wang, C.T., Wang, S.C. & Gao, N. 2015. Microhardness and corrosion properties of hypoeutectic Al-7Si alloy processed by high-pressure torsion. *Materials and Design* 83: 193-202. doi:10.1016/j.matdes.2015.06.018.

Xu, C. & Langdon, T.G. 2003. Influence of a round corner die on flow homogeneity in ECA pressing. *Scripta Materialia* 48(1): 1-4. doi:10.1016/S1359-6462(02)00354-8.

Xu, J., Shirooyeh, M., Wongsa-Ngam, J., Shan, D., Guo, B. & Langdon, T.G. 2013. Hardness homogeneity and micro-tensile behavior in a magnesium AZ31 alloy processed by equal-channel angular pressing. *Materials Science and Engineering: A* 586: 108-114.

Zheng, Z.J., Gao, Y., Gui, Y. & Zhu, M. 2012. Corrosion behaviour of nanocrystalline 304 stainless steel prepared by equal channel angular pressing. *Corrosion Science* 54(1): 60-67. doi:10.1016/j.corsci.2011.08.049.

Zhilyaev, A.P. & Ruano, O.A. 2011. Influence of the supersaturated silicon solid solution concentration on the effectiveness of severe plastic deformation processing in Al-7 wt.% Si casting alloy. *Materials Science and Engineering: A* 528(27): 7938-7947. doi:10.1016/j.msea.2011.07.016.

Zhu, M. 2017. Effects of T6 heat treatment on the microstructure, tensile properties, and fracture behavior of the modified A356 alloys. *Journal of Materials & Design* 36(November): 243-249. doi:10.1016/j.matdes.2011.11.018.

M.A. Gebril* & M.Z. Omar
Centre for Materials Engineering and Smart Manufacturing
Universiti Kebangsaan Malaysia
43600 UKM Bangi, Selangor Darul Ehsan
Malaysia

M.A. Gebril*
Department of Mechanical Engineering
Faculty of Engineering
Benghazi University, Benghazi
Libya

N.K. Othman
School of Applied Physics
Faculty of Science and Technology
Universiti Kebangsaan Malaysia
43600 UKM Bangi, Selangor Darul Ehsan
Malaysia

I.F. Mohamed
Fuel Cell Institute
Universiti Kebangsaan Malaysia
43600 UKM Bangi, Selangor Darul Ehsan
Malaysia

*Corresponding author; email: gebril.ukm@gmail.com